Original Research Article

# Evaluation of a complementary metal oxide semiconductor detector as a tool for stereotactic body radiotherapy plan quality assurance

Chris J. Stepanek [*], Jackie A. Haynes, Sally Fletcher

*Department of Radiotherapy, Bristol Haematology & Oncology Centre, University Hospitals Bristol & Weston NHS Foundation Trust, Horfield Road, Bristol BS2 8ED, United Kingdom*

ARTICLE INFO

ABSTRACT

*Background and purpose:* A sub-mm resolution Complementary Metal Oxide Semiconductor sensor has been developed for stereotactic radiotherapy quality assurance. Herein we evaluate its basic dosimetric performance and its application for linac C-arm stereotactic body radiotherapy (SBRT) plan quality assurance.
*Materials and methods:* The detector was integrated into its accompanying phantom or in Water Equivalent Plastic (WEP). The measurement reproducibility, stability, dose linearity and dependence on angularity, dose rate and field size were investigated. Clinical plan measurements were compared to our radiotherapy treatment planning system and radiochromic film. Sensitivity to introduced Multi Leaf Collimator (MLC) offsets was evaluated by simulating single MLC offsets in SBRT plans and comparing measurements to expected doses.
*Results:* Signal reproducibility was within $\pm$ 0.1 % and output calibration was stable over a 6 month period. Detector showed good linearity with dose ($r^2 = 1$). Signal decreased by 5 % when dose rate was decreased from 1300 MU/min to 300 MU/min. Output factors agreed within 0.5 % of chamber measurements for 1x1 cm field sizes or greater. Angularity measurements showed good agreement with reference. For measurement of planned clinical doses, gamma pass-rates were 98.5 % $\pm$ 2.3 % (treatment planning system reference, 2 %/2mm) and 99.2 % $\pm$ 1.0 % (film reference, 2 %,2mm). The detector also showed sensitivity to errors of 1 mm offsets in MLC positioning.
*Conclusion:* The detector performed well when used for pre-treatment SBRT plan quality assurance, offering a good alternative to radiochromic film.

## 1. Introduction

Stereotactic Body Radiotherapy (SBRT) treatments are characterised by a high dose per fraction, steep dose gradients and small radiation fields. High dose rate Flattening Filter Free (FFF) radiation beams are often used, and treatments may be delivered using coplanar or non coplanar beam arrangements or Volumetric Modulated Arc Therapy (VMAT). This poses challenges to achieving reliable and sufficiently accurate pre treatment verification of planned radiation doses [1–5]. Radiochromic film is often considered the detector of choice for SBRT verification, as no volume averaging effects are observed due to its high spatial resolution [6]. Measurements are also independent of dose rate, energy and angularity [7]. However, film exposure and processing can be very labour intensive and require careful calibration, storage and handling [8]. A recent report demonstrated favourable accuracy of a set of synthetic diamond detectors for point dose measurements in

stereotactic radiation fields [9]. However, single element sensors provide very little information about the broader dose distribution.

The need to develop 2D and 3D radiation detectors with significantly greater spatial resolution has prompted a move towards solid state and liquid filled detector arrays, which contain smaller sensor elements but are still capable of generating large magnitude signals. This has resulted in a small range of digital commercial devices suited to pre treatment verification of stereotactic radiotherapy treatment plans. Characterisation of these detectors in stereotactic radiation beams has been recently reported [10–12], and their suitability for Patient Specific Quality Assurance (PSQA) has been demonstrated for Cyberknife® Stereotactic Radiosurgery (SRS) [13] as well as linac based SRS [14,15] and SBRT [16,17]. These devices have spatial resolutions of ~ 2.5 mm. Due to the finite detector size, volume averaging and interpolation between sensor elements is required, which adds measurement uncertainty. Recent publications have demonstrated promising results for the use of

complementary metal oxide semiconductor (CMOS) technology for radiation dosimetry [18,19]. This has led to the commercial clinical release of a detector consisting of 100,000 CMOS elements with an effective spatial resolution of 0.4 mm. This sensor provides continuous dose profiles without the need for significant volume averaging or dose interpolation between the sensor elements. Its application for PSQA has been demonstrated for Cyberknife® SRS [20]. Our work evaluates the clinical CMOS detector's performance for C-arm linac SBRT plan quality assurance.

We report the detector's basic dosimetric properties including signal reproducibility and stability, relationship between signal reported and dose, dose rate, field size (through measurement of output factors) and angularity. To assess clinical dose measurement performance, 22 SBRT plan doses of 6 MV FFF energy were measured and compared to those calculated using our Treatment Planning System (TPS) and measured using radiochromic film. Additionally, SBRT plans containing a single introduced MLC offset were measured and compared to the calculated doses using gamma analyses for a range of clinically relevant gamma parameters to characterise the detector's sensitivity.

## 2. Materials & methods

Computed Tomography (CT) scans were acquired using a Philips BigBore CT Scanner. Treatment plans were produced using Raystation version 7.0 or version 10.0 (RaySearch Laboratories, Sweden) using the RaySearch collapsed cone convolution algorithm with a 0.1 cm resolution dose grid. Radiation was generated by 5 matched Elekta Versa HD Linear Accelerators using clinical beams of energy 6 MV FFF (TPR$_{20/10}$ = 0.679).

The myQA SRS Detector and Phantom are products of IBA Dosimetry (Schwarzenbruck, Germany). Sensor size is $12 \times 14$ cm, sensor element size is $0.4 \times 0.4$ mm and spatial resolution is 0.4 mm leaving no spacing between elements. The detector is inserted into a cylindrical phantom with a diameter of 19 cm with a hemispherical end for non-coplanar cranial treatments. The phantom is composed of Acrylonitrile butadiene Styrene (density = 1.06 g/cm$^3$) where the centre of the CMOS detector is positioned at 9.5 cm depth and may be replaced with film or chamber inserts. Film dosimetry was performed using EBT3 film (Ashland Speciality Ingredients). Films were scanned using an Epson X10000 Scanner and analysed using myQA Patients. For ion chamber dosimetry, an NE2571 Farmer chamber (sensitive volume = 0.6 cm$^3$), CC04 chamber (IBA Dosimetry, volume = 0.04 cm$^3$) and a Razor chamber (IBA Dosimetry, volume = 0.01 cm$^3$) were used.

### 2.1. Basic dosimetric performance

For reproducibility, the % deviation between six successive measurements relative to the first measurement was reported. For stability, output calibration factors acquired each month were compared to previous months. For dose linearity, the CMOS detector and a Farmer chamber were irradiated simultaneously. The CMOS detector was set up with an SSD of 100 cm, measurement depth of 6.7 cm in WEP, and the ion chamber was positioned with its sensitive volume on the central axis downstream of the CMOS detector. The Farmer chamber signal was used to correct detector signal to account for any non linearity in the output of the linear accelerator. For each measurement, the normalised detector signal from a central 4 mm × 4 mm Region of Interest (ROI) was used for our reported values. For dose rate dependence, the detector and a Farmer chamber were set up as for dose linearity measurements. The signal reported from a central 4 mm × 4 mm detector ROI was compared to signal from the Farmer chamber. Signals were normalised to the signal at the maximum nominal dose rate. Dose Per Pulse (DPP) dependence was studied according to the method used by Biasi et al. [21]. Briefly, the detector was set up at 5 cm depth in WEP, and average CMOS detector readings to a central 4 × 4 mm ROI were reported for various SSDs to modulate dose per pulse. These measurements were

replicated using a farmer chamber, and a ratio of CMOS reading/chamber reading was used to define the detector's DPP sensitivity. Measurements for ion recombination effects at each DPP were performed according to the two voltage method [22]. DPP values were calculated by scaling a literature value for a Elekta versa 6MV FFF [23] by ion chamber ratios measured under reference and our conditions. For field size dependence, output factors were measured using the CMOS detector and compared to corresponding measurements made using a Farmer chamber from 10x10cm to 5x5cm, a CC04 chamber from 5x5cm to 2x2cm and using a Razor chamber from 2x2cm to 0.5x0.5 cm. Detectors were positioned at 95 cm SSD and 5 cm depth in WEP under full scatter conditions and 100 MUs were delivered. Three sets of measurements were performed for each field size. For field sizes smaller than 3x3cm, beam profiles were acquired using the Razor chamber with a Blue Phantom Smartscan Watertank (IBA Dosimetry) to position the chamber at the centre of the profile. For angular dependence, the CMOS detector was integrated into the SRS Phantom, positioned at machine isocentre and exposed to 100 Monitor Units (MU), 6 MV FFF, 4 cm × 4 cm beam. The average signal to a central 4 mm × 4 mm ROI was recorded for each measurement and was normalised to the signal measured for the exposure at 0° gantry angle. These data were compared to the angular correction data provided by IBA.

### 2.2. Clinical dose measurement

A total of 22 coplanar VMAT SBRT plans for various anatomical sites (lung, spine, prostate, nodes and liver) were recalculated onto the CT volume of the CMOS detector and CMOS phantom using a 1 mm dose grid. An appropriate isocentre for each plan was chosen and the plans were then delivered to the CMOS detector within the phantom. Measurements were acquired at a frame rate of 2 frames per second and corrected for uniformity, output and angularity. A gantry angle sensor was used to report the incident beam angle required for the angular correction of each frame whilst the detector remained stationary. For analysis, the align data tool within the myQA software was used to remove any additional translational offsets between the planned/film and CMOS doses. Subsequently, a global gamma analysis was performed. For plan measurements using film, the film insert was inserted into the phantom (replacing the detector) prior to the exposure.

### 2.3. Sensitivity to MLC offsets

The sensitivity of the detector was investigated by studying its ability to detect dose differences corresponding to incorrect MLC configurations within SBRT treatment plans. For four SBRT treatment plans, a single MLC leaf within the target was withdrawn by 1, 2 or 5 mm to simulate the mis calibration of a crucial MLC. Doses from unmodified plans and plans with an introduced offset were calculated using the TPS and measured using the CMOS detector integrated into the phantom. Doses calculated for plans with introduced offsets were compared with doses calculated for unmodified plans to produce a 'calculated gamma map' for each introduced offset. This provided the TPS's estimation of the effect of the offset MLC on dose delivered. Similarly, doses measured for plans with introduced offsets were compared with doses measured for unmodified plans to produce a 'measured gamma map' for each offset. This provided the detector's estimation of the effect of the MLC offset on dose delivered. Doses measured using the CMOS detector for all plans were compared to TPS doses for the unmodified plans using a range of clinically relevant gamma parameters. To establish the clinical effect of these offsets, plan Conformity Indices (CI) were calculated according to the UK SABR Consortium guidelines [24].
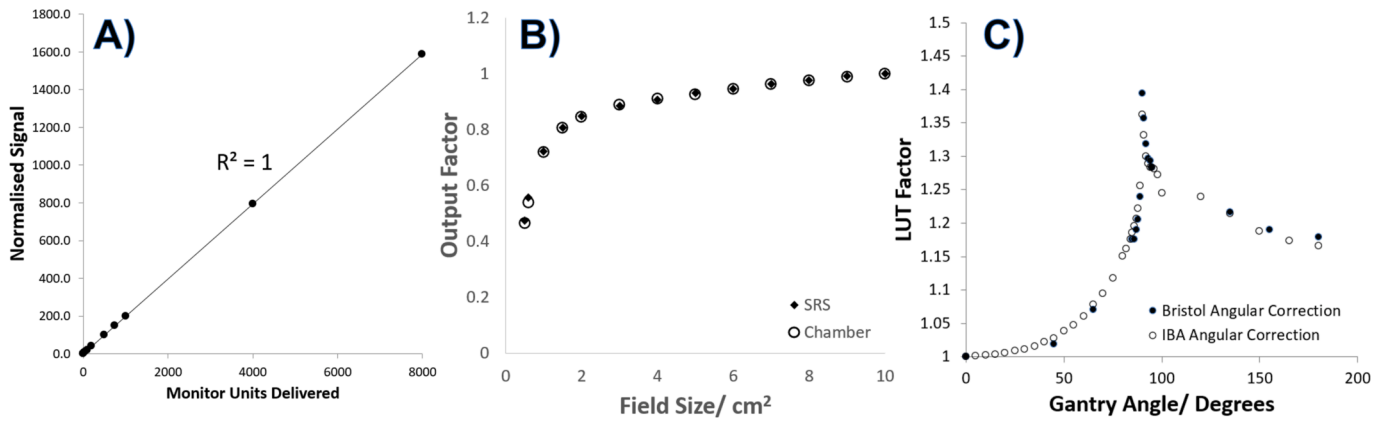
**Fig. 1.** Assessment of the detector's basic dosimetric response to 6 MV FFF beams. A) dose linearity. B) Field size dependence and C) angular dependence as a function of gantry angle. The software's default angular correction values are also shown and normalised to the value used when the detector is perpendicular to the incident beam (gantry angle = 0°).
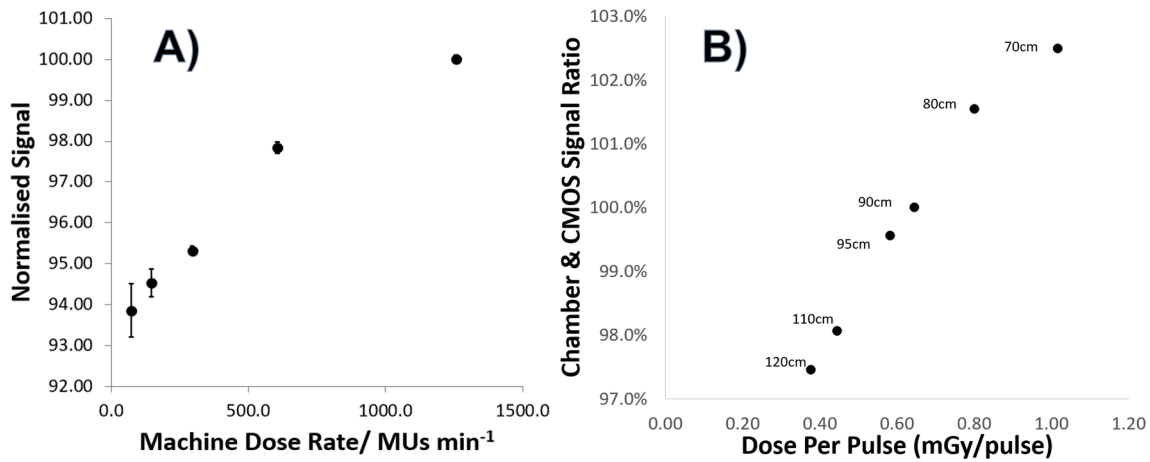


**Fig. 2.** Further assessment of the detector's basic dosimetric response to 6 MV FFF beams. A) dose rate dependence (error bars show ±1 standard deviation, n=3), B) Dose Per Pulse dependence within the range of SSDs 70cm to 120cm. Corresponding SSDs shown.

## 3. Results

### 3.1. Basic detector performance

The detector signal was within 0.1 % of the baseline signal, and the detector did not report significant background signal. Measured output calibrations were typically valid for up to 6 months post measurement. As shown in Fig. 1.A, the detector showed a linear response with dose ($R^2 = 1$), and the difference between the detector signal and the chamber signal was at most 1.4 % over 5 – 8000 MU. Fig. 1.B shows the output factors measured using the detector agreed well with chamber measurements. Factors corresponding to field sizes of 1 cm × 1 cm or larger were within 0.5 % of chamber doses, and factors corresponding to 0.5 cm × 0.5 cm and 0.6 cm × 0.6 cm differed by 2.6 % and 3.4 %, respectively. The detector shows a non-isotropic response as a function of incidence angle (Fig. 1.C), with signal from beams delivered at close to 90° relative to the plane of the detector requiring the most significant correction. When angular correction was applied to the signals measured at each gantry angle, the maximum difference between the signal measured at Gantry Angle = 0° and all other signals was −2.3 %, and the average percentage difference was 0.0 % ± 1.2 %.

Fig. 2.A shows the detector's recorded signal increased with increasing dose rate, and this dependence was most pronounced at lower dose rates. For instance, at a dose rate of 350 MU/min, the dose reported by the detector was 95.3 % of the dose reported at the maximum dose

**Table 1**
Gamma pass rates for all 6MV FFF SBRT plans when compared to planning dose distributions.

| Treatment Site | Couch moves/ cm | γ Pass Rates (%) | | | |
|---|---|---|---|---|---|
| | | 3 %, 3 mm | 2 %, 2 mm | 1 %, 1 mm | 3 %, 1 mm |
| Prostate | 0 | 99.8 | 98.9 | 95.3 | 96 |
| Spine | 0 | 100 | 99.9 | 88.1 | 99.4 |
| Spine | 0 | 99.5 | 95.5 | 72.9 | 91.2 |
| Pelvic Node | 5 Lt | 100 | 99.6 | 92 | 98.4 |
| Prostate | 0 | 99.7 | 99.5 | 92.4 | 99.9 |
| Para Aorta | 3 Ant | 100 | 100 | 100 | 100 |
| Liver | 2 Lt, | 100 | 99.4 | 87.6 | 99.7 |
| Aortic Node | 3 Ant | 100 | 99.7 | 60.5 | 95.9 |
| Pelvic Node | 3 Rt | 100 | 100 | 86.8 | 96.1 |
| Prostate | 0 | 100 | 99.8 | 83.2 | 99.9 |
| Adrenal | 3 Lt | 100 | 99.8 | 92.4 | 99.8 |
| Sacrum | 3 Rt, 6 Pos | 99.9 | 96.2 | 72.7 | 93.1 |
| Iliac Node | 4 Lt | 100 | 100 | 93.5 | 100 |
| Liver | 9 Ant | 99.4 | 98.3 | 86.6 | 97.3 |
| Liver | 3 Pos | 99.3 | 94.9 | 75.6 | 95.3 |
| Liver | 5 Lt, 1 Inf | 99.9 | 96.3 | 59.3 | 97.1 |
| Lung | 7 Lt, 5 Pos | 100 | 99.7 | 91.5 | 99.9 |
| Lung | 6 Rt, 5 Pos | 100 | 99.6 | 84.1 | 98.8 |
| Lung | 3 Lt, 3 Pos | 100 | 99.9 | 94.8 | 99.5 |
| Lung | 7.5 Rt, 8 Pos | 99.6 | 91.3 | 51.6 | 90.5 |
| Spine | 0 | 100 | 97.8 | 74.8 | 92.2 |
| Spine | 0 | 100 | 100 | 93.7 | 98.7 |
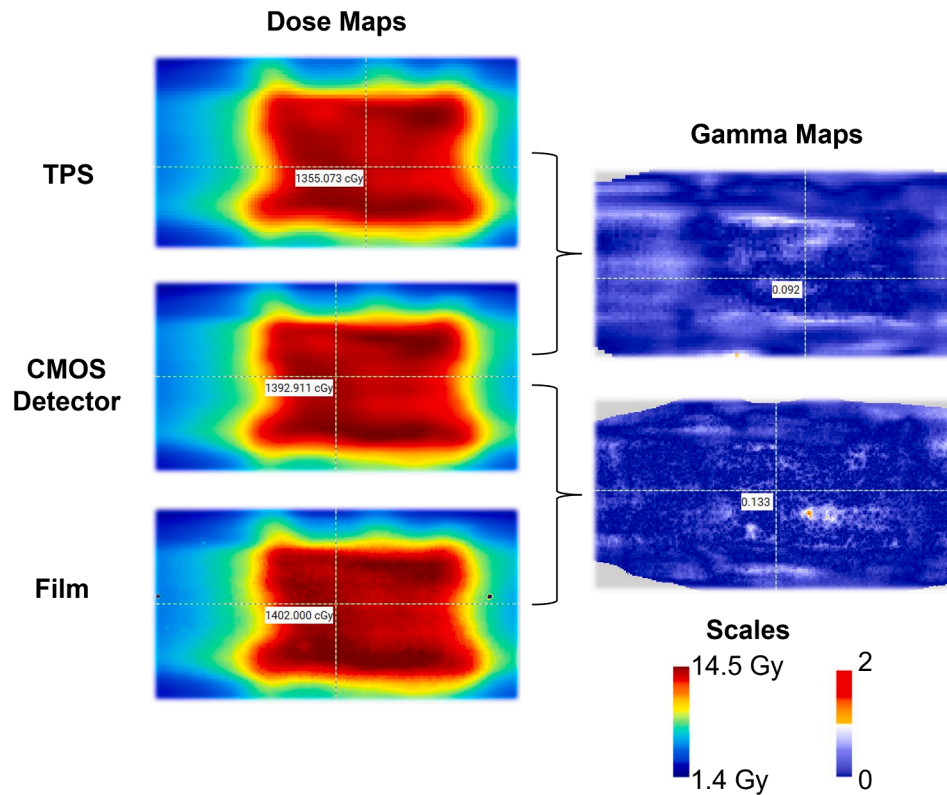
**Fig. 3.** Coronal dose distribution of a 6 MV FFF SBRT spine plan measured by the CMOS detector, calculated using the TPS and measured using film. Corresponding global gamma analysis comparisons comparing CMOS doses to TPS and film doses are also shown (2%/2mm,15% threshold).
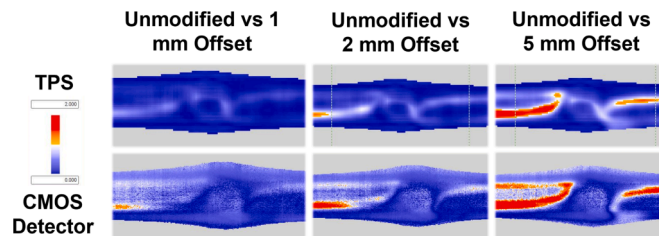


**Fig. 4.** Calculated and measured gamma maps comparing the sensitivity of the TPS and the CMOS detector to introduced single 1, 2 and 5 mm MLC offsets for a 6 MV FFF SBRT node plan. Gamma parameters were 1%/1mm, 15% threshold.

rate (1300 MU/min). Fig. 2.B shows a 5 % variation in DPP sensitivity across the DPP range of 0.38 – 1.02 mGy/pulse which corresponds to SSDs of 70 cm to 120 cm. Variation in $k_{ion}$ across this range of DPP was within 0.25 %.

### 3.2. Clinical plan measurement

The mean gamma pass rates comparing calculated and measured doses for all 22 plans, were 98.5 % $\pm$ 2.3 % and 97.2 % $\pm$ 3.1 % for 2 %/2mm and 3 %/1mm, respectively. Individual pass rates for all SBRT plans studied are shown in Table 1. Fig. 3 shows the dose distribution from an SBRT spine plan measured by the CMOS detector, calculated by the TPS and measured by film. Gamma analyses comparing the detector and film measurements following the delivery of 7 SBRT 6MV FFF plans provided mean pass rates of 98.3 % $\pm$ 2.0 % and 96.6 % $\pm$ 3.1 % for 2 %/2mm and 3 %/1mm, respectively.

### 3.3. Sensitivity to MLC offsets

Fig. 4 shows calculated and measured global gamma maps comparing a 6 MV FFF SBRT node plan with the same plan modified to contain single MLC offsets of 1 mm, 2 mm and 5 mm, respectively. This figure is representative of all four plans studied. Amongst the gamma maps of these dose distributions the effect of the withdrawn MLC can clearly be seen by the red band of failure, which increases in size with increasing offset.

Fig. 5 shows the sensitivity of the CMOS detector to single MLC offsets as a function of offset size and choice of gamma parameters. When gamma parameters of 3 %/3mm were used, the detector was only sensitive to the 5 mm introduced offsets. When gamma parameters 2 %/2mm or smaller were used, it was sensitive to all offsets. However, for gamma parameters smaller than 2 %/2mm, the average pass rate for the unmodified plans also dropped markedly and pass rate variation significantly increased. Overall, clear reductions in gamma pass rate were observed with increasing MLC offset, which corresponded to an increase in Planning Target Volume (PTV) mean dose and mean CI (an increase of 2.1 % and 0.08, respectively, were observed for a 5 mm introduced offset). Increasing CI corresponds to a decreased level of conformity as CIs for all unmodified plans were greater than 1.

### 4. Discussion

The CMOS detector's dose linearity is comparable to that reported for other devices, and results were acquired through similar methodologies (although not all studies used FFF beams) [11,12,20]. Signal reproducibility was similar to that reported elsewhere for Cyberknife® beams [20]. Dose rate dependence was consistent with other reports of the same device [20], and greater than that reported for the SRS MapCheck, for which deviations of < 0.5 % compared to a chamber have been reported for a similar range of dose rates [11,14]. Our linacs
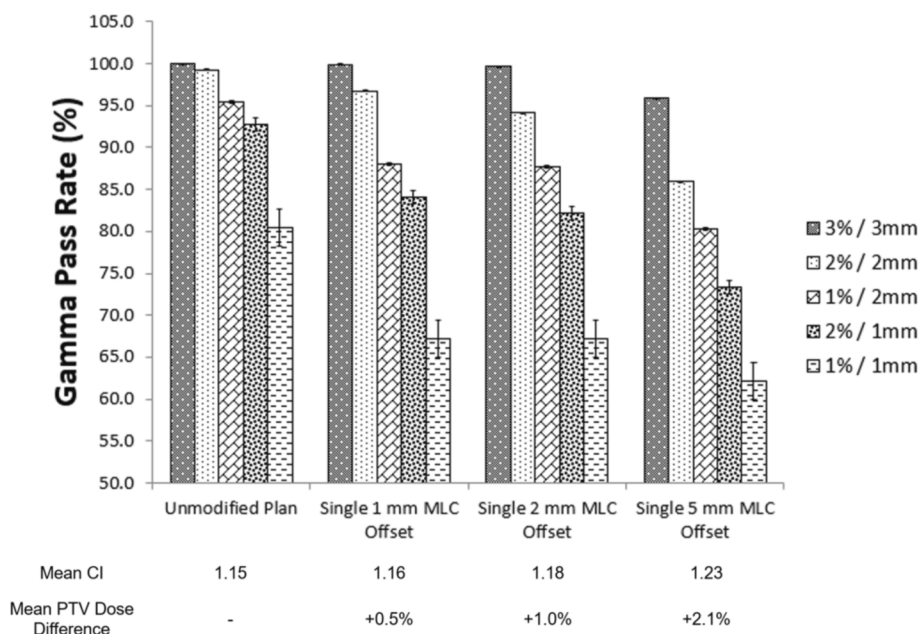
**Fig. 5.** Mean gamma pass rates for four SBRT plans with no introduced MLC offset, as well as introduced 1mm, 2mm and 5mm single MLC offsets. Measured doses were compared to TPS doses for the original plan. Results were analysed using five combinations of global % dose difference and distance to agreement (mm) parameters. Error bars represent ± 1 standard deviation unit across three technical repeats. Also included, calculated changes in mean CI and mean PTV dose corresponding to increased MLC offset.

delivered almost all the MUs of our SBRT plans at dose rates exceeding 1000 MU/min, reducing the significance of this dependency. CMOS signal decreased with decreasing DPP, a behaviour observed for detectors of similar composition [25]. This sensitivity variation was ± 2.5 % across the range we studied, which is similar to comparable devices for 6 MV FFF [21]. Due to the geometry of the phantom and isocentric VMAT nature of the plans, DPP effects would generally not be significant but should be considered when interpreting measurements with large offsets. The CMOS detector showed a similar field size dependence to the SRS Mapcheck [14] and the PTW Octavius [12] for a similar range of field sizes. Typically, these devices measure output factors within 1 % of ion chamber measurements down to field sizes of 1 cm × 1 cm or 0.5 cm × 0.5 cm, at which deviations of 2–3 % are observed [10,12,14]. The CMOS detector showed an angular dependence like that observed for the Octavius 1000 SRS [12] and the SRS Mapcheck [14] for equivalent energies and similar field sizes. All these devices have methods of correcting for this non isotropy, such as gantry mounted inclinometers, which either apply a direct correction to measured signal or facilitate the rotation of the detector such that it is always perpendicular to the gantry. We concluded the CMOS detector's gantry angle sensor provided sufficient angular correction to measured doses.

The detector demonstrated very good agreement with film and TPS for the measurement of SBRT doses, indicating the detector's dose rate and DPP dependence weren't significant. Literature examples of similar detectors used for stereotactic radiotherapy PSQA employed a variety of delivery techniques such as static IMRT fields [17], non coplanar arcs [15], mixture of coplanar and non coplanar arcs [14,16] and Cyberknife deliveries [13,20]. Furthermore, several treatment sites were studied including brain lesions [13–15,20] and a range of SBRT sites [16,17]. These studies used tight gamma parameters to analyse their dose planes due to the greater importance of dosimetric accuracy for stereotactic treatments. We favoured the use of 2 %/2mm due to the high agreement between the CMOS detector, film & planning system as well as the small variation in pass rates. Although these parameters were also favoured in other articles [17], our results demonstrated that the use of 3 %/1mm would also be suitable for this detector, as was used in other publications [13–16]. Literature pass rates for VMAT QA delivered by a C-arm linac using these devices were 98.9 % using the MapCheck (3 %/1mm, n = 6) [14], 96.0 % also for the MapCheck (3 %/1mm, n = 32) [16] and 99.3 % for the Octavius (3 %/1mm, n = 15) [15]. These are comparable to the CMOS detector pass rates and suggests that sample size as well as range

of treatment sites and delivery styles are an important consideration when attempting to interpret these statistics. Our measured pass rates were significantly greater than the rates reported for the same detector when used to measure significantly non coplanar Cyberknife® deliveries [20].

The use of gamma parameters 2 %/2mm offered good sensitivity to MLC offsets with minimal variation. The detector's resolution provides clear visualisation of the gamma map manifestation of the MLC errors. This is a very useful visual aid to assist the operator in diagnosing a mis calibrated MLC, which reenforces the benefits of careful inspection of pairs of dose distributions and their corresponding gamma maps to assist the investigation of suspicious results. Similar work has been published for the Octavius 1000 SRS [26]. In this study, MLC offsets of up to 0.5 mm were introduced into intracranial SRS plans. These offsets were applied to half the MLCs on the X1 and X2 banks. These MLC errors resulted in a reduction in gamma pass rates, but in terms of clinical significance, the effect on Mean PTV dose was small (<2%) and the effect on CI was inconclusive. Our observed increases in Mean PTV dose difference and CI suggest single MLC offsets of the magnitudes studied could have a significant clinical impact. The UK SABR Consortium recommends CIs for SBRT plans to be within the range 1.1 – 1.25, depending on target volume size [24]. Clearly however, the detector's ability to detect MLC offsets having clinical significance depends on the original plan, it's quality and department tolerances.

We conclude that the CMOS detector provides a good alternative to film for SBRT QA, having provided consistent clinical dose measurements without requiring inter element dose interpolation or significant volume averaging. The detector also shows promise for being sensitive to MLC offsets that could result in clinically significant dose differences.

### Declaration of Competing Interest

The authors declare the following financial interests/personal relationships which may be considered as potential competing interests: We would like to acknowledge that this project was sponsored by IBA Dosimetry (Germany), who also provided technical help when required. IBA Dosimetry did not however, conduct any arbitration of our work.

### Acknowledgements

## References

[1] Lo SS, Fakiris AJ, Chang EL, Mayr NA, Wang JZ, Papiez L, et al. Stereotactic body radiation therapy: a novel treatment modality. Nat Rev Clin Oncol 2010;7:44–54. https://doi.org/10.1038/nrclinonc.2009.188.

[2] Timmerman RD, Kavanagh BD, Cho LC, Papiez L, Xing L. Stereotactic body radiation therapy in multiple organ sites. J Clin Oncol 2007;25:947–52. https://doi.org/10.1200/JCO.2006.09.7469.

[3] Andreo P. The physics of small megavoltage photon beam dosimetry. Radiother Oncol 2018;126:205–13. https://doi.org/10.1016/j.radonc.2017.11.001.

[4] Aspradakis MM, Byrne JP, Palmans H, Conway J, Rosser K, Warrington JAP. Small field MV photon dosimetry. first ed. York, UK: IPEM; 2010. IPEM report 103.

[5] Lo SS, Foote M, Siva S, Slotman BJ, Teh BS, Guckenberger M, et al. Technical know-how in stereotactic ablative radiotherapy (SABR). J Med Radiat Sci 2016;63:5–8. https://doi.org/10.1002/jmrs.163.

[6] Fuss M, Sturtewagen E, De Wagter C, Georg D. Dosimetric characterization of GafChromic EBT film and its implication on film dosimetry quality assurance. Phys Med Biol 2007;52:4211–25. https://doi.org/10.1088/0031-9155/52/14/013.

[7] Gonzalez-Lopez A, Vera-Sanchez JA, Lago-Martin JD. Small fields measurements with radiochromic films. Med Phys 2015;40:61–7. https://doi.org/10.4103/0971-6203.158667.

[8] Soares CG. Radiochromic film dosimetry. Radiat Meas 2006;41:100–16. https://doi.org/10.1016/j.radmeas.2007.01.007.

[9] Shaw M, Lye J, Alves A, Keehan S, Lehmann J, Hanlon M, et al. Characterisation of a synthetic diamond detector for end to end dosimetry in stereotactic body radiotherapy and radiosurgery. Phys Imaging Radiat Oncol 2021;20:40–5. https://doi.org/10.1016/j.phro.2021.10.002.

[10] Shukaili KA, Petasecca M, Newall M, Espinoza A, Perevertaylo VL, Corde S, et al. A 2D silicon detector array for quality assurance in small field dosimetry: DUO. Med Phys 2017;44:628–36. https://doi.org/10.1002/mp.12060.

[11] Yasui K, Saito Y, Ogawa S, Hayashi N. Dosimetric characterization of a new two-dimensional diode detector array used for stereotactic radiosurgery quality assurance. Int J Radiat Res. 2021; 19: 281-89. doi: 10.3390/cancers7030844.

[12] Markovic M, Stathakis S, Mavroidis P, Jurkovic IA, Papanikolaou N. Characterization of a two-dimensional liquid-filled ion chamber detector array used for verification of the treatments in radiotherapy. Med Phys 2014;41:051704. https://doi.org/10.1118/1.4870439.

[13] Xu Q, Huynh K, Nie W, Rose MS, Chawla AK, Choe KS, et al. Implementing and evaluating a high-resolution diode array for patient-specific quality assurance of robotic brain stereotactic radiosurgery/radiotherapy. J Appl Clin Med Phys 2022; 23:13569.

[14] Ahmed S, Zhang G, Moros EG, Feygelman V. Comprehensive evaluation of the high-resolution diode array for SRS dosimetry. J Appl Clin Med Phys 2019;20: 13–23. https://doi.org/10.1002/acm2.12696.

[15] McCulloch J, Pawlowski J, Kirby N, Rasmussen K, Shi Z, Myers P, et al. Patient-specific dose quality assurance of single-isocenter multiple brain metastasis stereotactic radiosurgery using PTW Octavius 4D. J Appl Clin Med Phys 2020;21: 107–15. https://doi.org/10.1002/acm2.12979.

[16] Rose MS, Tirpak L, Van Casteren K, Zack J, Simon T, Schoenfeld A, et al. Multi-institution validation of a new high spatial resolution diode array for SRS and SBRT plan pretreatment quality assurance. Med Phys 2020;47:3153–64. https://doi.org/10.1002/mp.14153.

[17] Markovic M, Narayanasamy G, Stathakis S, Mavroidis P, Jurkovic IA, Saenz D, et al. Clinical evaluation of a two-dimensional liquid-filled ion chamber detector array for verification of high modulation small fields in radiotherapy. Med Phys 2019;44:91–8.

[18] Spang FJ, Rosenberg I, Hedin E, Royle G. Photon small-field measurements with a CMOS active pixel sensor. Phys Med Biol 2015;60:4383–98. https://doi.org/10.1088/0031-9155/60/11/4383.

[19] Beck L, Velthuis JJ, Fletcher S, Haynes JA, Page RF. Using a TRAPS upstream transmission detector to verify multileaf collimator positions during dynamic radiotherapy delivery. Appl Radiat Isot 2020;156:108951. https://doi.org/10.1016/j.apradiso.2019.108951.

[20] Padelli F, Aquino D, Fariselli L, De Martin E. IBA myQA SRS detector for cyberKnife robotic radiosurgery quality assurance. Appl Sci 2022;12:7791. https://doi.org/10.3390/app12157791.

[21] Biasi G, Petrasecca M, Guatelli S, Hardcastle N, Carolan M, Perevertaylo V, et al. A novel high-resolution 2D silicon array detector for small field dosimetry with FFF photon beams. Phys Med 2018;45:117–26. https://doi.org/10.1016/j.ejmp.2017.12.010.

[22] Eaton DJ, Bass G, Booker P, Byrne J, Duane S, Frame J, et al. IPEM code of practice for high energy photon therapy dosimetry based on the NPL absorbed dose calibration service. Phys Med Biol 2020;65:195006. https://doi.org/10.1088/1361-6560/ab99e3.

[23] Xiao Y, Kry SF, Popple R, Yorke E, Papanikolaou N, Stathakis S, Xia P, Huq S, Bayouth J, Galvin J, Yin FF. Flattening filer free accelerators: a report from the AAPM therapy emerging technology assessment work group. J Appl Clin Med Phys. 2015; 16: 12-29 doi: 10.1120%2Fjacmp.v16i3.5219.

[24] UK SABR consortium. Stereotactic Ablative Body Radiation Therapy (SABR): A Resource (Version 6.1). Brentford, UK: SABR consortium; 2019.

[25] Rikner G, Grussel E. Effects of radiation damage on p-type silicon detectors. Phys Med Biol 1983;28:1261–7. https://doi.org/10.1088/0031-9155/28/11/006.

[26] O'Connor P, Seshadri V, Charles P. Detecting MLC errors in stereotactic radiotherapy plans with a liquid filled ionization chamber array. Australas Phys Eng Sci Med 2016;39:247–52. https://doi.org/10.1007/s13246-016-0421-6.